There was supposed to be an asteroid-shattering kaboom!: Benchmarking the *Rebound* Ejecta Dynamics package with asteroid impact simulations J. Larson[1] and G. Sarid[2,3,4], [1]Department of Physics, University of Central Florida, [2] Science Systems and Applications, [3]SETI Institute, [4]Florida Space Institute.

Introduction: Debris ejected off small bodies, whether by impact or activity-driving processes (sublimation, fission, etc.), provide insight and constraints on the physical evolution and chemical constitution of small bodies' surfaces and sub-surfaces. Typically debris clouds are modeled using hydrodynamic simulations that approximate debris cloud evolution based on gradients across the cloud [1,2]. While this method reduces the required computational resources, the types of simulated systems available using the hydrodynamic method is much more limited than an N-body approach that traces individual particle interactions [3]. Using the N-body particle approach, we can model the microdynamics of a particle cloud with varied particle size and velocity distributions as well as trace collisions between individual particles within the cloud.

The Python implementation of *Rebound* [4] makes it possible to do N-body calculations at a higher temporal resolution at a lower performance cost than most commonly used schemes [5]. In addition, *Rebound* offers a collision function that allows for particle-particle interactions [4]. While other N-body codes, such as PKDGRAV [6], are used in specific ejecta dynamics simulations, these integrators demand high computational requirements and long simulation times [5]. The *Rebound* Ejecta Dynamics package (RED) described here can increase the computational speed and reduce the CPU hours required for each simulation.

Here we expand on our previous implementations and benchmarking of RED as applied to two types of asteroid systems [7,8]: a main belt asteroid (such as (596) Scheila [9,10]) and a binary asteroid system (such as the Didymos system [11]). We discuss here the effects that are currently implemented, a few results with those two asteroid systems, and our upcoming work.

Methodology: Effects implemented in this current package version include a particle size and initial velocity distributions, radiation pressure, a binary component, small body rotation, and ellipsoidal gravitational potential. Initially, we test each effect individually in order to explore the influence of each effect independently of other effects. Each effect is tested on a main belt asteroid and a binary asteroid system. We chose (596) Scheila as our main belt asteroid since extensive observations of a post-impact debris cloud off of this asteroid exist [9,10]. While it is not our primary objective here to reproduce imaging of the (596) Scheila debris cloud, we use the observations as a baseline for how particles should interact with a main belt asteroid. Secondly, we apply these effects to possible debris clouds in the Didymos system as an analog for a binary asteroid system. The Didymos system is the target for the Double Asteroid Redirection Test (DART) impact which aims to impact the system's secondary body in an attempt to demonstrate the deflection of an asteroid [11].

For these benchmarking simulations, we start the debris cloud near the equator with a direct collision, perpendicular to the surface, defining an opening angle of 45° for the benchmarking simulations. The initial particle velocity distribution is defined by [1,12] and illustrated in fig. 1 with an initial particle speed of 70% the escape velocity. The initial input speed is multiplied by the normalized velocity factor (y-axis) that corresponds to the particle's radius from the center of the ejecta cone (x-axis). The benchmark simulations implement a uniform size distribution unless specified otherwise.

The varied particle size distribution is required for the implementation of solar radiation pressure. We implement a power law distribution similar to [13] with a large number of small particles (10^{-4} m) and a few large particles (1 m). We apply the radiation pressure as a force that acts on small particles to push them away from the sun.

Additionally, we include an ellipsoidal gravitational potential for the asteroids. Rather than using the spherical potential to approximate an ellipsoid, we expand the ellipsoidal gravitational potential equation given by [14]. Rotation about the principal axis provides a shift in the gravitational potential over time [14]. This potential is extended to any secondary or tertiary components in the system. We benchmark the binary system against the Didymos system using spherical bodies initially. Once interactions in a binary asteroid system has been tested with spherical bodies, we include ellipsoidal bodies.

Results: We first benchmark this package with the Didymos system and an impact on (596) Scheila by simulating clouds with no additional effects. Here the particles are lofted above the surface and expand evenly from the center of the cloud. If the initial particle velocity is above the escape velocity then the particles will not fall back upon the surface; particles slower than the escape velocity will fall on the surface.

When including a particle size distribution, the simulation results do not alter from the no effects scenario unless radiation pressure is also included. This

effect acts most strongly on smaller particles as shown in fig. 2, which shows the ratio of radiation pressure to gravitational acceleration for different particle sizes at varying heights above a 100km radius body. In our benchmark simulations, smaller particles drift along a vector pointing away from the sun. The effect is not strong in systems farther than 2AU from the sun.

Next, we include ellipsoidal gravitational potential. Particles drift towards the regions of higher gravitational potential on either end of the longest axis. The rotation of the primary body increases the amount of drift due to the included centripetal force acting perpendicular to the axis of rotation.

Finally, we add a spherical binary to a system with a spherical target body to benchmark a binary asteroid system. Particles ejected from the surface nearest the binary will follow the gravitational pull of the binary as shown in fig. 3.

Upcoming Work: The results presented here are merely examples of each implemented effect for the purpose of benchmarking; however, next we will apply this package to several planetary science questions. Our two main future applications for this package are preliminary modeling for the DART mission impact and to test the long-term evolution of debris as a result of an impact or activity on a Centaur.

Due to the increased computational speed of *Rebound*, we are able to produce a large library of results in a much sorter time than other N-body codes. This is quite useful for preliminary modeling efforts for the DART impact. As part of our future work, we are creating a library of possible short-, medium-, and long-term ejecta evolution simulations.

Finally, we test the evolution of debris around a Centaur object under various conditions. Many Centaurs have cometary activity and outbursts [15] that require modeling to determine how this debris interacts with the Centaurs. In addition, a couple Centaurs have been observed with thin rings [16], yet the origins of these rings are still unknown. We will use RED to test the likelihood that these rings could have formed from the long-term evolution of surface debris.

The beta version of RED will be published [17] to the *Rebound* repository for public use by April 2020.

References: [1] Housen K. R. et al. (1983). J. Geophys. Res., 88, 2485–2499. [2] Holsapple K. R. (1993). Ann. Rev. Earth Planet. Sci., 21, 333–373. [3] Artemieva N. (2008) Large Meteorite Impacts and Planet. Evo. IV, 3082. [4] Rein H. and Liu S.-F. (2012) *A & A, 537,* A128. [5] Rein H. and Tamayo D. (2017) *Mon. Not. R. Astron. Soc.* [6] Stadel J. G. (2001) PhD Thesis, Univ. of Washington. [7] Larson J. and Sarid G. (2017) LPS XLVIII, 2829. [8] Larson J. and Sarid G. (2018) LPS XLIX, 2083. [9] Jewitt D. et al. (2011) *ApJ Letters*, *733,* L4. [10] Ishiguro M. et al. (2011) *ApJ Letters, 741*, L24. [11] Cheng A. F. et al. (2016) *Planet. & Space Sci., 121,* 27-35. [12] Cintala M. J. et al. (1999) *Meteorit. Planet. Sci., 34,* 605-623. [13] O'Brian D. P. and Greenberg R. (2003) *Icarus, 164*, 334. [14] Hu X., (2017) *AJ, 850,* 107. [15] Jewitt D. (2009) *AJ*, *137,* 4295-4312. [16] Braga-Ribas F. et al. (2014) *Nature, 508,* 72-75. [17] Larson J. and Sarid G. (2019) *MNRAS,* Under Review.

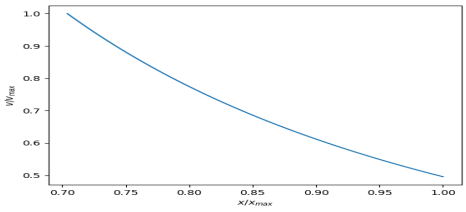

Figure 1. The normalized velocity distribution function at each radius from the cone's center. The initial input speed is multiplied by the normalized velocity fraction at corresponding distances from the center.

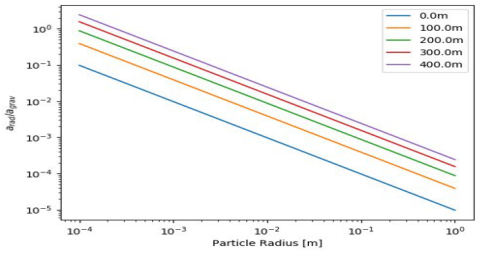

Figure 2. Here we show the ratio of gravitational acceleration to radiation pressure acceleration for varying particle radii. Each line represents a different distance from the surface of a 100km radius body at 1AU.

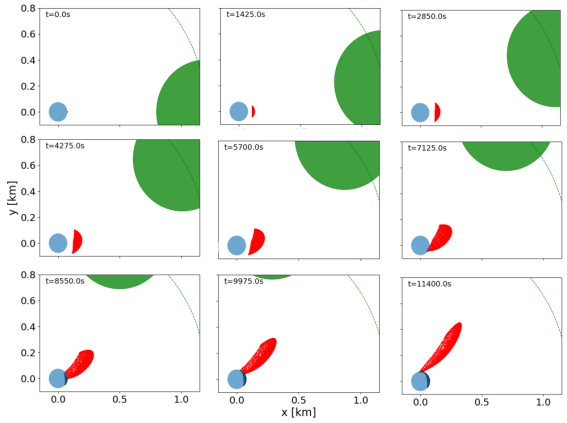

Figure 3. The Didymos system is simulated with 10^4 particles and spherical bodies. Particles are ejected at 70% the escape velocity of Didymoon and drift towards the secondary component over time.